ADVANCES IN ATMOSPHERIC SCIENCES, VOL. 33, JUNE 2016, 673–684

Ensemble Simulation of Land Evapotranspiration in China Based on a Multi-Forcing and Multi-Model Approach

Jianguo LIU[1,2], Binghao JIA[*2], Zhenghui XIE[2], and Chunxiang SHI[3]

[1]*High Performance Computing Center, School of Mathematics and Computational Science, Huaihua University, Huaihua, Hunan* 418008

[2]*State Key Laboratory of Numerical Modeling for Atmospheric Sciences and Geophysical Fluid Dynamics, Institute of Atmospheric Physics, Chinese Academy of Sciences, Beijing* 100029

[3]*National Meteorological Information Center, China Meteorological Administration, Beijing* 100081

(Received 7 October 2015; revised 25 December 2015; accepted 20 January 2016)

ABSTRACT

In order to reduce the uncertainty of offline land surface model (LSM) simulations of land evapotranspiration (ET), we used ensemble simulations based on three meteorological forcing datasets [Princeton, ITPCAS (Institute of Tibetan Plateau Research, Chinese Academy of Sciences), Qian] and four LSMs (BATS, VIC, CLM3.0 and CLM3.5), to explore the trends and spatiotemporal characteristics of ET, as well as the spatiotemporal pattern of ET in response to climate factors over mainland China during 1982–2007. The results showed that various simulations of each member and their arithmetic mean (Ens_Mean) could capture the spatial distribution and seasonal pattern of ET sufficiently well, where they exhibited more significant spatial and seasonal variation in the ET compared with observation-based ET estimates (Obs_MTE). For the mean annual ET, we found that the BATS forced by Princeton forcing overestimated the annual mean ET compared with Obs_MTE for most of the basins in China, whereas the VIC forced by Princeton forcing showed underestimations. By contrast, the Ens_Mean was closer to Obs_MTE, although the results were underestimated over Southeast China. Furthermore, both the Obs_MTE and Ens_Mean exhibited a significant increasing trend during 1982–98; whereas after 1998, when the last big EI Niño event occurred, the Ens_Mean tended to decrease significantly between 1999 and 2007, although the change was not significant for Obs_MTE. Changes in air temperature and shortwave radiation played key roles in the long-term variation in ET over the humid area of China, but precipitation mainly controlled the long-term variation in ET in arid and semi-arid areas of China.

Key words: land evapotranspiration, ensemble simulations, multi-forcing and multi-model approach, spatiotemporal variation, uncertainty

Citation: Liu, J. G., B. H. Jia, Z. H. Xie, and C. X. Shi, 2016: Ensemble simulation of land evapotranspiration in China based on a multi-forcing and multi-model approach. *Adv. Atmos. Sci.*, **33**(6), 673–684, doi: 10.1007/s00376-016-5213-0.

1. Introduction

Land surface evapotranspiration (ET), i.e., the sum total of water transferred from the land surface to the atmosphere, plays vital roles in the global hydrological cycle, energy balance, and carbon cycle during land–atmosphere interactions within the climate system (i.e., latent heat flux) (Dirmeyer, 1994; Jung et al., 2010; Wang and Dickinson, 2012; Shi et al., 2013). Water exchange returns about 60% of the precipitation on the land surface to the atmosphere, which then affects the local climate (Oki and Kanae, 2006). Thus, it is very important to quantify the spatiotemporal patterns and changes in regional ET to understand the interactions between the land surface and atmosphere by monitoring the land surface conditions that force extreme events, such as drought and flood, as well as evaluating the potential impact on climate change (Xu et al., 2006; Gao et al., 2007; Bonan, 2008; Jung et al., 2010).

Four methods are used to obtain ET estimates: ground-based observations, the water balance method (Gao et al., 2007, 2012), satellite retrieval (Chen et al., 2014; Li et al., 2014; Mao et al., 2015), and land surface modeling (Chen et al., 2013; Shi et al., 2013), where each has its own advantages and disadvantages (Wang and Dickinson, 2012). For example, ground-based observations can provide high quality ET records with high temporal resolution, but they have a short duration and sparse spatial coverage. Satellite retrieval can characterize the spatial variability of ET well, but these data cannot be used to establish the relatively long-term climate variability in ET. Previously, there have been few studies of long-term regional ET, and most have focused on the water

* Corresponding author: Binghao JIA
Email: bhjia@mail.iap.ac.cn

balance method (Gao et al., 2007, 2012); however, it is difficult to derive a significant trend of ET from water balance because (1) there is large interannual variability of precipitation and inconsistencies between different data sources, and (2) the river discharge directly flowing into oceans is difficult to estimate (Wang and Dickinson, 2012).

At present, land surface models (LSMs) are used widely to obtain ET estimates at global and continental scales because of their mechanism-based structure (Vinukollu et al., 2012; Chen et al., 2013; Jaksa et al., 2013; Shi et al., 2013; Mao et al., 2015); however, LSM simulations of ET still contain many errors (Dirmeyer et al., 2006; Wang and Dickinson, 2012). The main sources of error in offline LSM simulations of ET are the uncertainties in meteorological forcing and those in the land surface parameterizations. The accuracy of a simulation based on an LSM depends mainly on the quality of the meteorological forcing and the land surface parameterization scheme (Dirmeyer et al., 1999; Wang and Zeng, 2011; Chen et al., 2013). Multiple-LSM ensembles have been found to perform significantly better than a single LSM at land surface modeling, as well as reducing the uncertainties in the land surface parameterizations (Guo et al., 2007). Similar findings have been reported for meteorological forcing (Liu and Xie, 2013).

However, previous studies of the spatiotemporal patterns and changes in regional ET have focused mainly on simulations by single LSMs (Shi et al., 2013) or multiple LSM simulations driven by a single meteorological dataset (Chen et al., 2013, Mao et al., 2015). Such work does not consider the uncertainties from the atmospheric forcing dataset and the land surface parameterizations, simultaneously. Therefore, in this study, we used three meteorological forcing datasets to drive four LSMs, to reduce both types of uncertainties in ET. The three meteorological forcing datasets were developed by Sheffield et al. (2006) at Princeton University (hereafter, Princeton), He (2010) at the Institute of Tibetan Plateau Research, Chinese Academy of Sciences (hereafter, ITPCAS), and Qian et al. (2006) (hereafter, Qian). For the offline LSM simulation, four widely used LSMs were adopted in this study: (1) BATS (Dickinson et al., 1993; Giorgi et al., 2003); (2) VIC (Liang et al., 1996; Liang and Xie, 2001; Mitchell et al., 2004); (3) CLM3.0 (Oleson et al., 2004); and (4) CLM3.5 (Oleson et al., 2007). First, six simulations based on the four LSMs and driven by the three meteorological forcing datasets were conducted for mainland China. Next, the six sets of simulated ET data were merged by simply using the arithmetic average, and a comparison was conducted among the six simulations, ensemble simulations, and global land ET data, which were derived from the FLUXNET network of eddy covariance towers using the model tree ensembles (MTE) approach (Obs_MTE) (Jung et al., 2009, 2010). Furthermore, we analyzed the trends and spatiotemporal characteristics of ET over mainland China and the eight major river basins of China. Finally, we considered the spatiotemporal patterns in ET in response to climatic factors.

The remainder of the paper is organized as follows: In section 2, we provide brief descriptions of the three types of meteorological forcing, as well as the four LSMs, the Obs_MTE data, and the experimental design. In section 3, we compare the Obs_MTE data with individual and ensemble simulations of ET, as well as illustrate the trends and spatiotemporal characteristics in ET, and the spatiotemporal patterns of ET in response to climatic factors over mainland China and the eight major river basins of China. We discuss the results in section 4 and finally provide a summary and give our conclusions in section 5.

2. Models, data and method

2.1. *Multiple types of meteorological forcing*

Offline LSM modeling requires external meteorological forcing data, and thus the accuracy of LSM modeling depends largely on the quality of meteorological forcing, where it is especially sensitive to precipitation, radiation, and temperature (Wei et al., 2008; Wang and Zeng, 2011). The external meteorological forcing data used to drive offline LSMs include the air temperature, wind speed, specific humidity, surface pressure, precipitation, and radiation. In this study, we used three sets of meteorological forcing data over mainland China, which were developed by different institutions to drive LSMs, as follows:

(1) The Princeton meteorological forcing dataset, which combines the NCEP–NCAR reanalysis dataset (Kalnay et al., 1996) and a suite of global observation-based products. The observation-based products comprise the CRU TS2.0 product, the GPCP precipitation product, the TRMM precipitation product, and the NASA Langley Research Center SRB product. Sheffield et al. (2006) described the details of this dataset, while Sheffield and Wood (2007) used this dataset to evaluate the global terrestrial water budget. In addition, Wang et al. (2011) used this dataset to drive four different physical-based LSMs to explore soil moisture drought in China.

(2) The ITPCAS forcing dataset, which is a hybrid of data obtained from the GLDAS dataset (Rodell et al., 2004) [the old version used the Princeton global meteorological forcing data as background data (Sheffield et al., 2006)] and a suite of observation-based products from China. Specifically, it combines the GLDAS dataset with observations from 740 operational stations of the China Meteorological Administration (CMA) to produce near-surface air temperature, pressure, wind speed, and specific humidity fields, as well as three merged precipitation datasets to determine the precipitation field. In addition, the corrected GEWEX-SRB (Pinker and Laszlo, 1992) shortwave radiation dataset, with reference to radiation estimates (Yang et al., 2006), is employed to ascertain the incident shortwave radiation fields. Chen et al. (2011) used the old version to investigate the land surface temperature in dryland areas of China.

(3) The Qian forcing dataset, which combines NCEP–NCAR reanalysis data and observation-based analyses of monthly precipitation, surface air temperature, and surface downward solar radiation. Details of the dataset, which was initially available for the period 1948–2004, are described

in Qian et al. (2006). Later, Tian et al. (2010) extended this dataset up to 2010 by using ERA-Interim data along with the precipitation and temperature records from 740 CMA operational stations. They then employed the dataset to develop a land data assimilation system.

Table 1 summarizes the primary features and the differences between the forcing data.

2.2. *Multiple LSMs*

In this study, we employed four widely used LSMs (including a macroscale hydrological model)—BATS, VIC, CLM3.0 and CLM3.5—to model land ET over mainland China. These LSMs have been used in previous offline land surface modeling experiments, and their performances evaluated. In these LSMs, ET is parameterized as the sum of vegetation evaporation, vegetation transpiration, and soil evaporation. Spatial land surface heterogeneity in the four LSMs is represented as a subgrid hierarchy in which grid cells are composed of multiple snow/soil columns, plant function types, or other surface types. Biogeophysical progresses are simulated at the subgrid scale, and each subgrid unit maintains its own prognostic variables (e.g., ET). However, the same forcing is used to force all subgrid units within a grid cell. Finally, the grid-averaged ET is obtained by averaging the subgrid values weighted by their fraction areas. Thus, the vegetation and soil parameters should be provided in each LSM and taken from the LSM's standard setup.

Table 2 summarizes the primary features and the differences between these LSMs, as well as the sources of the vegetation and soil parameters.

2.3. *Obs_MTE data*

Due to the lack of direct observations of ET, we used Obs_MTE data to compare and evaluate our seven ET simulations (i.e., six simple simulations and their ensemble simulation). The point-wise ET observations from the FLUXNET measurement sites were up-scaled with geospatial information obtained from satellite remote sensing and surface meteorological data using the MTE algorithm, which yielded the monthly ET at a spatial resolution of 0.5° during 1982–2010 (Jung et al., 2009, 2010), which we designated as Obs_MTE in this study. Jung et al. (2010) used this dataset to explore the recent decline in the global land ET and its possible explanations. Shi et al. (2013) also used this dataset to evaluate the ET simulated by CLM4, and to further investigate the spatiotemporal patterns in ET in response to multiple environmental factors.

2.4. *Simulation setup*

The six ET simulations were determined by four different LSMs (described in Table 2) driven by three different types of forcing (described in Table 1), which we coded as: (1) VIC_Prin (for the VIC model driven by Princeton forcing); (2) BATS_Prin (for the BATS model driven by Princeton forcing); (3) CLM3_Prin (for the CLM3.0 model driven by Princeton forcing); (4) CLM3.5_Prin (for the CLM3.5 model driven by Princeton forcing); (5) CLM3.5_Qian (for the CLM3.5 model driven by Qian forcing); and (6) CLM3.5_ITP (for the CLM3.5 model driven by ITPCAS forcing). In order to achieve an equilibrium state in the LSMs, the Princeton forcing was first used to drive CLM3.5 from 1948 to 2008,

Table 1. Comparison of the major features of the three sets of meteorological forcing data.

Forcing	Resolution	Coverage	Composition	Institution	References
Princeton	3-h, 1° × 1°	Global, 1948–2008	1. CRU TS2.0, GPCP, and TRMM precipitation product 2. Temperature and cloud cover from CRU TS2.0 3. NASA Langley SRB radiation product 4. NCEP–NCAR reanalysis data	Princeton	Sheffield et al. (2006)
ITPCAS	3-h, 0.1°×0.1°	(15°–55°N, 70°–140°E), 1979–2012	1. Near-surface air temperature, pressure, wind speed, specific humidity, and precipitation from 740 CMA operational stations 2. GLDAS dataset 3. TRMM3B42 and APHRODITE* precipitation product 4. GEWEX-SRB shortwave radiation data and radiation estimates from a hybrid radiation model	ITPCAS	He (2010); Rodell et al. (2004); Yang et al. (2006)
QIAN	3-h, 1.875° lon × 1.915° lat	Global, 1948–2004; (15°–55°N, 70°–140°E), 2004–10	1. NCEP–NCAR reanalysis data 2. ERA-Interim data 3. Precipitation from Chen et al. (2002) and GPCP from Adler et al. (2003) 4. Temperature from Jones and Moberg (2003) and New et al. (1999) 5. Surface solar radiation from Zhang et al. (2004) and GEBA 6. Near-surface air temperature and precipitation in China from 740 CMA operational stations	NCEP IAPCAS	Qian et al. (2006); Tian et al. (2010)

*Asian Precipitation-Highly Resolution Observational Data Integration Toward Evaluation of Water Resources.

Table 2. Comparison of the major features of LSM structures and hydrological schemes.

Model	Soil hydrology scheme	Vegetation/soil parameters	References
BATS	Including a vegetation layer, a snow layer and three soil layers: top soil with depth of 10 cm; soil in root zone with depth of 1 m, 1.5 m, or 2 m; deep soil with depth of 3 m. Surface runoff is a function of the soil moisture.	Vegetation and land use data from the global databases for climate studies developed by Matthews (1983). Soil parameters from the FAO.	Matthews (1983); Dickinson et al. (1993); Giorgio et al. (2003)
VIC	The total soil column is divided into three layers, where the thickness is specified differently cell by cell with a range from 0.8 to 3 m. Variable infiltration capacity curve for surface runoff. ARNO model for base flow and drainage driven by gravity.	Vegetation and soil parameters from North American Land Data Assimilation System (NLDAS).	Liang et al. (1996); Liang and Xie (2001); Mitchell et al. (2004)
CLM3.0	The total soil column of 0–3.43 m is divided into 10 layers, with variable thickness ranging from 0.0175 to 1.1370 m. A combination of the TOPMODEL and BATS runoff scheme.	Vegetation data based on one-year AVHRR data.	Oleson et al. (2004)
CLM3.5	Modified version of CLM3.0, where the hydrological modifications mainly include canopy interception, runoff water table depth, frozen soil, soil water availability, and soil evaporation.	Vegetation data from MODIS. Soil data from IGBP.	Oleson et al. (2004); Niu et al. (2007)

and the first files from 1 January 2009 were then saved and used to initialize all six simulations at the beginning of each of the six modeling processes. These simulations were all run at a resolution of $0.5^\circ \times 0.5^\circ$, and the forcing data were also interpolated to 0.5°. The six sets of modeled ET data were then merged using a simple arithmetical averaging ensemble method and designated as Ens_Mean.

2.5. *Evaluation method*

The evaluation method comprised the following steps:

(1) The Obs_MTE data were used to compare and evaluate the six simulations of ET and their ensemble simulation at a spatial resolution of 0.5° during 1982–2007 in China and the eight major basins of China. Figure 1 shows a map indicating the locations of the eight major basins in China.

(2) The linear regression method (e.g., Fu et al., 2008; Gao et al., 2012) was used to compute the temporal trends in ET in China and the eight major basins of China.

(3) The correlation coefficients (R) between ET and climate variables (temperature, precipitation, radiance, wind speed etc.) were calculated to explore the sensitivity of ET to climate change.

3. Results

3.1. *Spatial pattern of ET*

In order to ensure the credibility of the ensemble simulation of ET, we first compared the six simulations and their ensemble simulation of the mean annual ET with the Obs_MTE

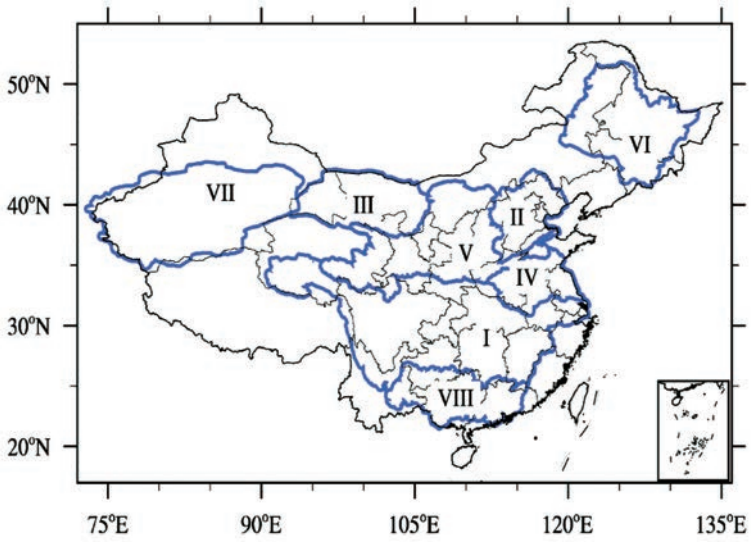

Fig. 1. Locations of the eight major river basins in China: I, Yangtze River basin; II, Haihe River basin; III, Heihe River basin; IV, Huaihe River basin; V, Yellow River basin; VI, Songhuajiang River basin; VII, Tarim River basin; and VIII, Zhujiang River basin.

data from 1982–2007 in China and the eight major basins of China (Fig. 2). Figure 2 shows that BATS_Prin overestimated the mean annual ET over most of the basins and all of China, whereas VIC_Prin obtained underestimates. The ensemble simulation Ens_Mean produced a closer simulation to the mean annual ET obtained with Obs_MTE data. The annual mean ET during the study period, over all of China, was simulated by Ens_Mean as 383 mm yr^{-1}, whereas the Obs_MTE estimate was 436 mm yr^{-1}.

Figure 3 shows the spatial distribution of the land annual-mean ET in China according to Obs_MTE, Ens_Mean, and the difference between them. Figure 3 demonstrates that the Obs_MTE data exhibited strong regional variations and there was an obvious southeast–northwest latitude gradient from high to low. In general, the lowest annual ET values were located in the arid/semiarid regions of Northeast China and Northwest China, such as the provinces of Xinjiang, Gansu, Inner Mongolia, and Ningxia (<400 mm yr^{-1}), whereas the annual ET values in South China were relatively high, such as in the provinces of Hainan, Taiwan, Yunnan, Guangxi, and Guangdong (>700 mm yr^{-1}) (Fig. 3a). The ensemble simulation Ens_Mean captured the spatial distribution of ET very well in China (Figs. 3a and b), but the Ens_Mean simulated ET was lower than that of the Obs_MTE over Southeast China (Fig. 3c), where the major contributor was the slightly lower Ens_Mean value estimated over all of China compared with the Obs_MTE data (Fig. 2).

From the perspective of hydrological basins, relatively high annual ET values were found for the Yangtze River, Zhujiang River, and Huaihe River basins, where the estimated ET ranged from 641 to 858 mm yr^{-1} (Fig. 2). In these humid subtropical basins, the temperature and moisture were sufficient to satisfy the vegetation ET and soil ET. Relatively low annual ET values were found in the Heihe River and Tarim River basins, where the estimates of ET ranged from 164 to 189 mm yr^{-1} (Fig. 2). In these cold and arid basins, moisture or temperature was the limiting factor. Intermediate annual ET values were found in the Huanghe River, Haihe River, and Songhuajiang River basins, where the estimates of ET ranged from 368 to 507 mm yr^{-1} (Fig. 2). In these temperate semihumid basins, the moisture and temperature levels were intermediate.

3.2. *Temporal variation in ET*

3.2.1. *Seasonal patterns of ET*

Figure 4 shows the multi-year seasonal pattern of land ET in China during 1982–2007 according to the Obs_MTE, Ens_Mean, and the difference between them. It can be seen that the Obs_MTE data exhibited obvious seasonal patterns, where the spatial variability was controlled by the climatic conditions. The highest ET values occurred in summer (June–

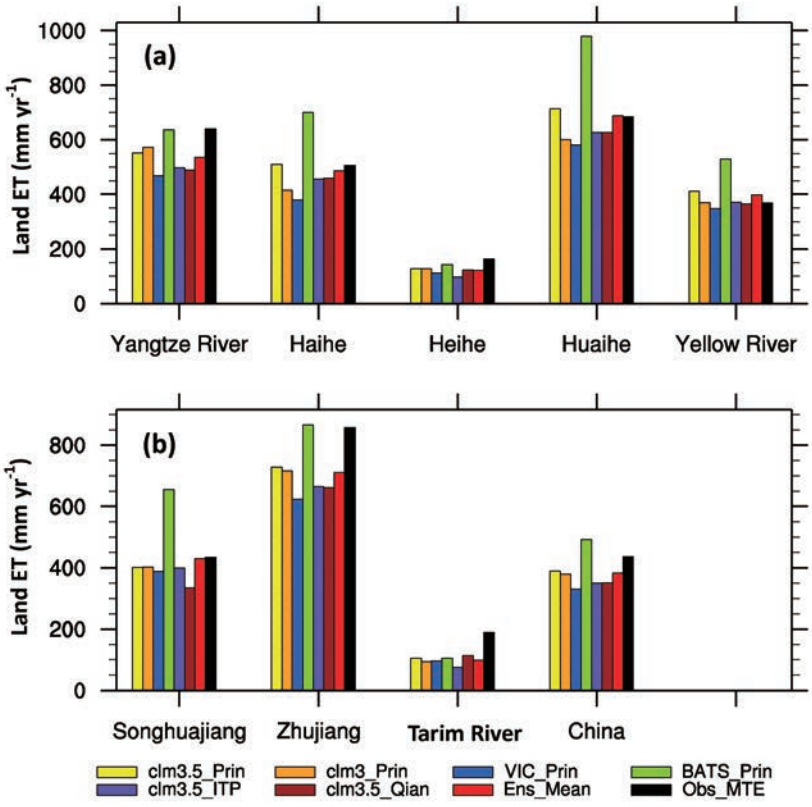

Fig. 2. Comparison of the average ET density (mm yr^{-1}) estimated for the eight major river basins of China, and all of China, based on multiple LSM simulations, Ens_Mean and Obs_MTE, during 1982–2007.

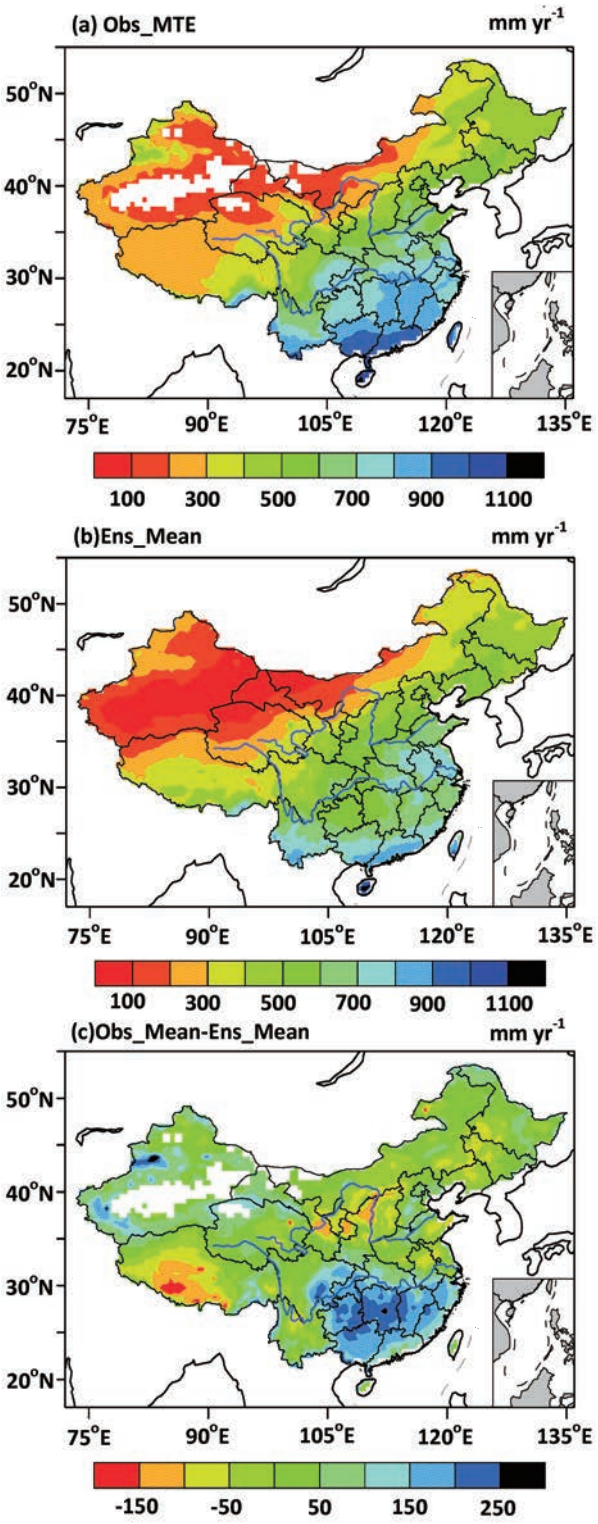

Fig. 3. Spatial distribution of the annual ET (mm yr^{-1}) during 1982–2007 (a) from Obs_MTE, (b) from Ens_Mean, and (c) the difference between Obs_MTE and Ens_Mean (i.e., Obs_MTE minus Ens_Mean). The white area in Northwest China represents the default Obs_MTE values.

August), where the most easterly and southern parts of China had the most striking high ET values, while there was an obvious spatial variation pattern where ET decreased from southeast to northwest. Relatively high ET values occurred in spring (March–May), whereas the lowest ET values occurred in winter (first column in Fig. 4). Thus, the moisture and the temperature were sufficient to satisfy ET over the southeast of China in the summer.

The ensemble simulation captured the seasonal pattern of ET in China very well (second column in Fig. 4), but the Ens_Mean simulated ET was lower than that of Obs_MTE over Southeast China (Fig. 4c), which was the major contributor to the slightly lower value of the Ens_Mean estimated for all of China compared with the Obs_MTE data.

3.2.2. *Time series*

In order to examine the performance of the ensemble-simulated ET quantitatively, we compared the Ens_Mean and Obs_MTE time series averaged over the eight major basins of China for 1991–2002 (Fig. 5). Figure 5 shows that the Ens_Mean captured the seasonal cycle and temporal evolution of Obs_MTE very well, but there were errors in some basins, such as those of the Heihe River, Zhujiang River, and Tarim River basins. The errors in the Heihe River basin may have been due to the greater human activity levels, such as land use, agricultural water use, and water use for environmental conservation. The errors in the Zhujiang River basin may have been due to complex surfaces, such as dense vegetation and complex terrain. There were large errors in the Tarim River basin (Obs_MTE higher than Ens_Mean), which were probably caused mainly by using the default Obs_MTE values in some areas of this basin because most of this area is desert and the ET values were very low.

3.2.3. *Interannual variation and temporal trend of ET*

Figure 6 shows the changes in Chinese annual land ET anomalies for both the Obs_MTE and Ens_Mean data from 1982 to 2007, which demonstrate that both the Obs_MTE and Ens_Mean exhibited significant interannual variability during this period. Relatively low values occurred in 1984, 1985, 2001 and 2003, whereas the highest values occurred in 1998. During 1982–98, the ensemble-simulated ET Ens_Mean values were generally consistent with the Obs_MTE data (R = 0.92, $P < 0.05$). After 1998, the Ens_Mean data exhibited more significant interannual variability than Obs_MTE, and they were not consistent.

On average, the Obs_MTE and Ens_Mean data exhibited a significant positive trend during 1982–98 (Obs_MTE: $y = x - 10.15$, $P < 0.05$; Ens_Mean: $y = 0.89x - 3.79$, $P < 0.05$). During 1998–2007, the Ens_Mean data exhibited a significant negative trend ($y = -2.19x + 3.24$, $P < 0.10$) and the Obs_MTE data also exhibited a negative trend ($y = -0.53x + 0.49$), but it was not significant. After 1998, when the last big EI Niño event occurred, the increasing trend in the land ET disappeared, and the subsequent declining trend was consistent with the Ens_Mean. This conclusion is consistent with the analysis of Obs_MTE for global ET data by Jung et al. (2010), but slightly different from the results based on eight satellite-based ET models (Chen et al., 2014), in which four of the eight models showed significant increases in ET, while

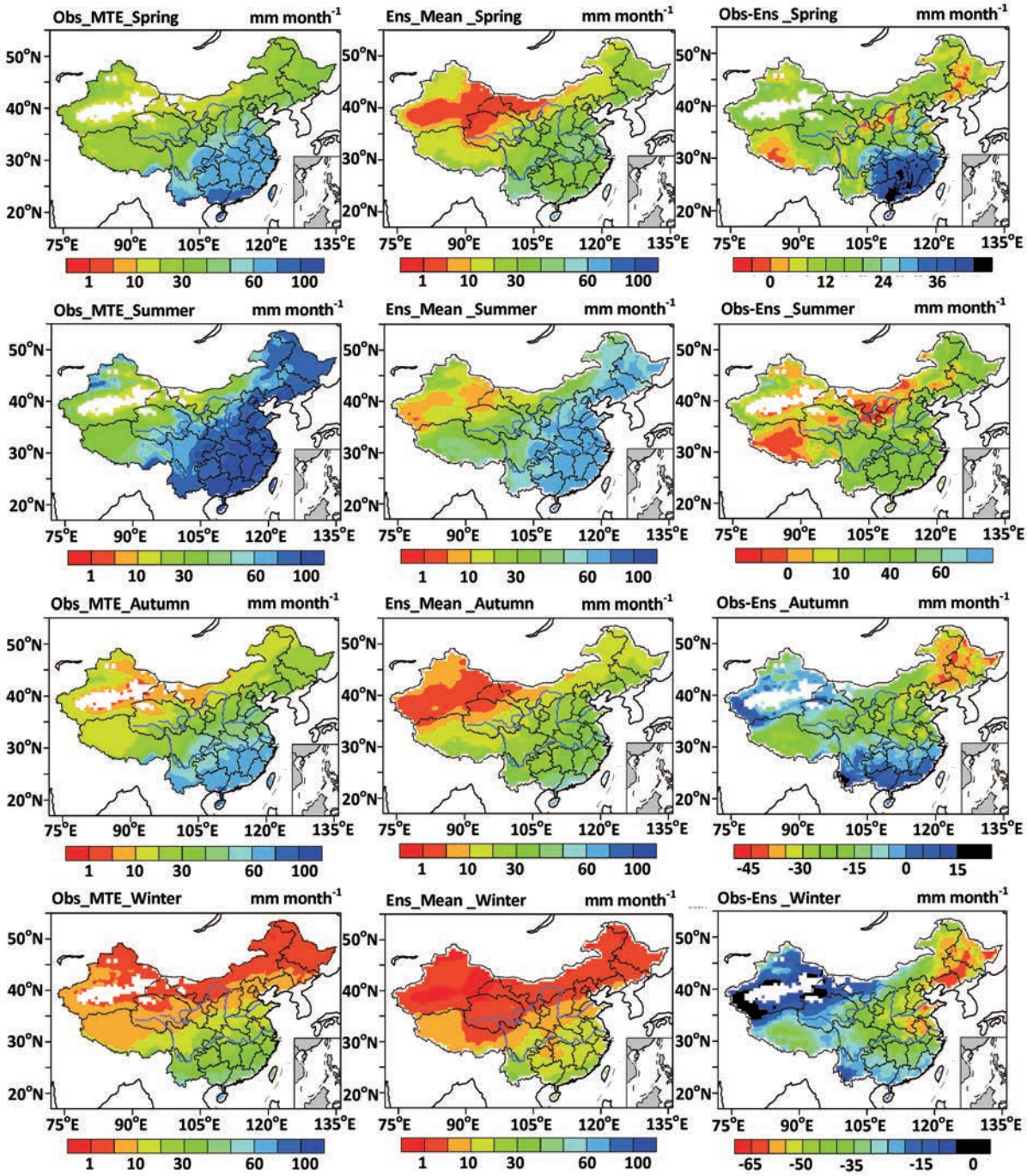

Fig. 4. Seasonal distribution of land ET (mm month^{-1}) in China during 1982–2007 obtained from Obs_MTE (first column), Obs_MTE (second column), and the difference between Obs_MTE and Ens_Mean (i.e., Obs_MTE minus Ens_Mean; third column). The white area in Northwest China represents the default Obs_MTE values.

the other models presented relatively constant long-term values, or slightly decreasing ET, over terrestrial ecosystems in China from 1982 to 2009. The differences in satellite-based ET model structure and their dominant variables were the major causes (Chen et al., 2014).

We also considered the regional-scale interannual variability in the land ET over the eight major basins of China. Figure 7 shows the temporal evolution of the annual land ET anomalies over the eight major basins of China, in terms of both the Obs_MTE and Ens_Mean, from 1982 to 2007. The results show that the Ens_Mean captured the basin-scale international variability in ET over the eight major basins in China, especially during 1982–1998, but the Ens_Mean exhibited more significant interannual variability compared with the MTE product. In 1998–2007, the Obs_MTE and Ens_Mean exhibited differences in their interannual variability

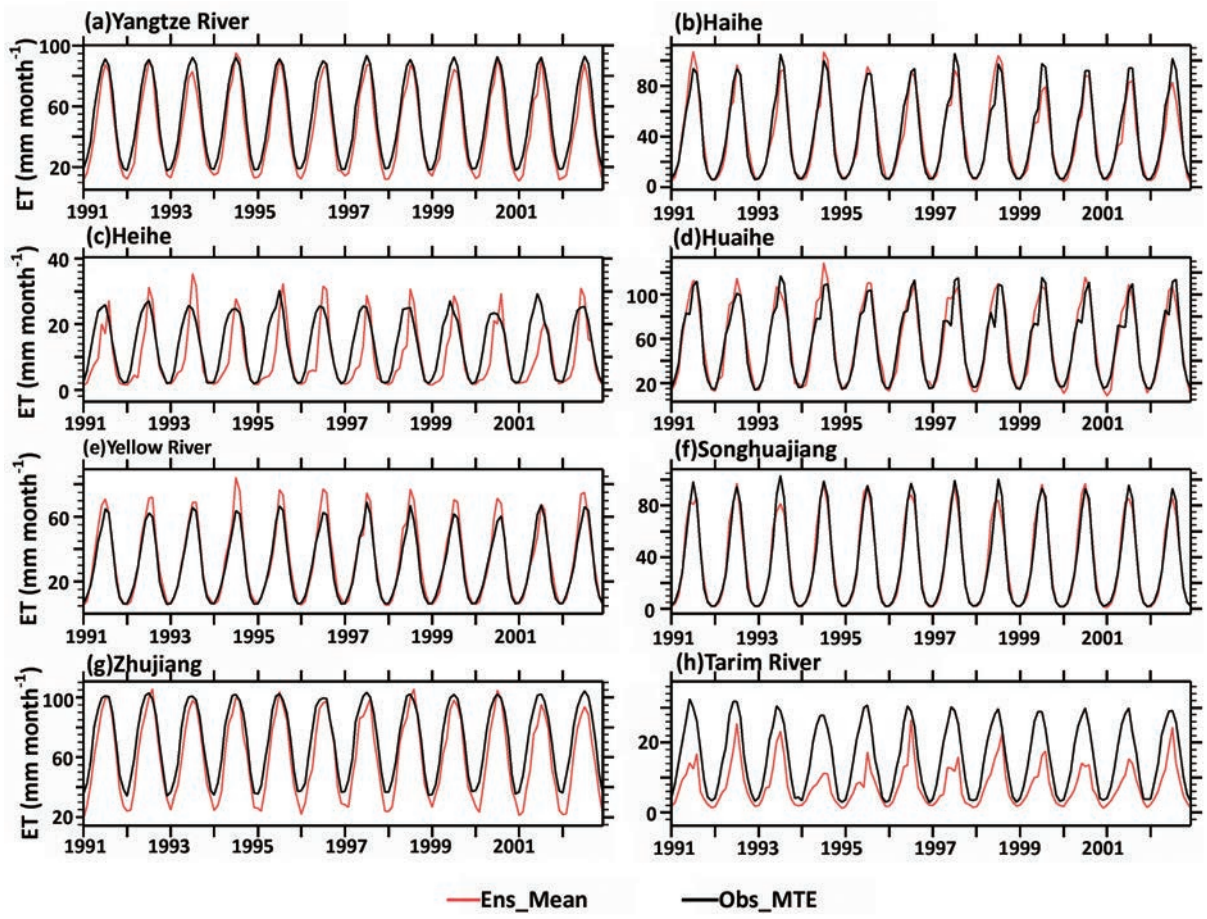

Fig. 5. Time series for land ET (mm month^{-1}) obtained from the Obs_MTE reported by Jung et al. (2009, 2010) and the Ens_Mean, for the eight major river basins of China.

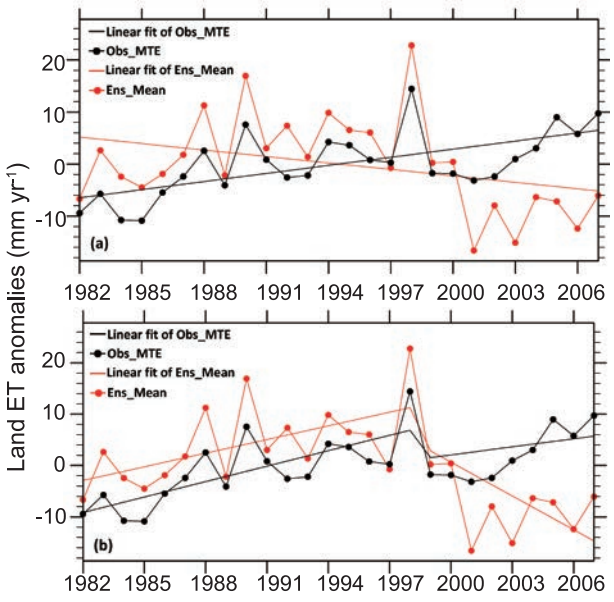

Fig. 6. Comparison of the differences in Chinese annual land ET anomalies between the Obs_MTE reported by Jung et al. (2009, 2010) and the Ens_Mean: (a) linear trend during 1982–2007; (b) linear trend during 1982–1998 and 1999–2007.

over most of the basins of China, and this conclusion is consistent with that over all of China.

3.3. *Sensitivity to climate change*

In order to explore the sensitivity of ET to climate change, we studied the relationship between ET and climate variability. Figure 8 shows the correlation coefficients for the relationships between ET and climate variability in China, i.e., air temperature (T_a), shortwave radiation (R_n), precipitation, and wind speed. In general, the results demonstrate T_a was the driver of ET over moist areas, with a significant positive correlation, e.g., in most parts of South China and some areas of Northeast China, where the correlation coefficients were lower in drier areas and negative over arid areas (Fig. 8b). We found a similar relationship between R_n and ET (Fig. 8c), but the positive correlation was more significant between T_a and ET. Precipitation controlled ET over dry areas, with a significant positive correlation, e.g., in most parts of Northwest China, where the correlation coefficients were lower in moister areas and zero or even negative for humid areas (Fig. 8d). There were few significant correlations between wind speed and ET in most parts of China, except the northwest of China (Fig. 8a). Thus, we found that the annual T_a and precipitation were important climate variables that affected the

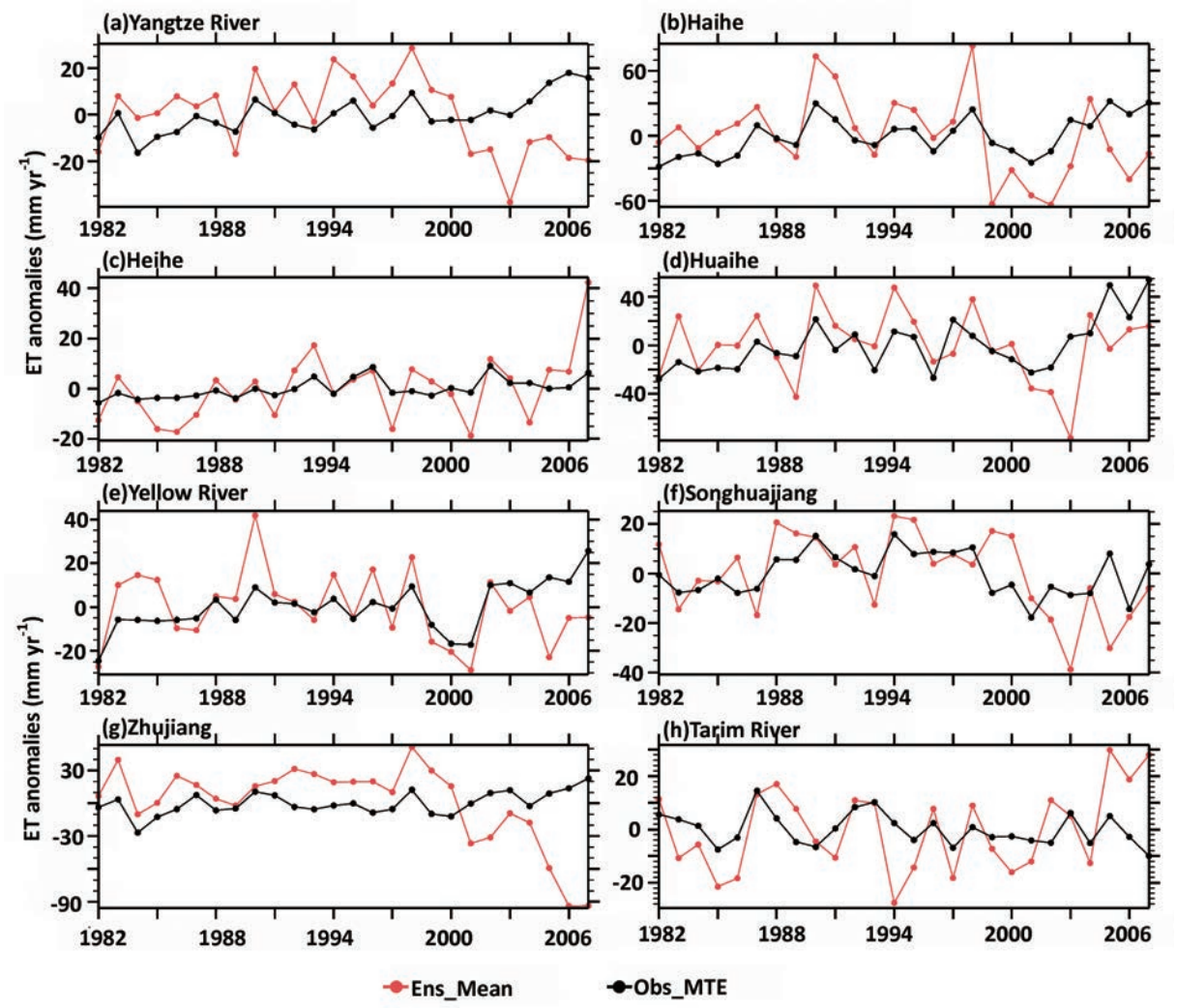

Fig. 7. Comparison of the differences in the annual land ET anomalies for the eight major basins between the Obs_MTE reported by Jung et al. (2009, 2010) and the Ens_Mean.

variation in ET, and there was a significant spatial pattern in the ET response to T_a and precipitation over mainland China during 1982–2007.

We further investigated the regional-scale relationship between ET and the important climate variables for the eight major basins of China. Table 3 shows the correlation coefficients for the relationships between ET and the climate variables (T_a and precipitation). These results demonstrate that ET had a significant positive correlation with T_a for most of the major basins in China, except the Tarim River basin and Heihe River basin, which are located in arid areas, and the correlation was higher for humid areas (e.g., the Yangtze River basin, Huaihe River basin, and Zhujiang River basin). Our conclusions were similar for the correlation between ET and R_n, but ET only had a significant positive correlation in humid areas (Yangtze River basin, Huaihe River basin, and Zhujiang River basin; not shown in Table 3), where T_a or R_n mainly controlled the long-term variation in ET in humid areas, and these conclusions agree with those of Wang et al. (2010) and Li et al. (2014). ET and precipitation were positively correlated in arid and semi-arid areas (Heihe River basin, Tarim River basin, Haihe River basin, Yellow River

Table 3. Correlations (R) between mean annual ET and climate variables (Air temperature and Precipitation) for the eight major river basins of China.

	Air temperature		Precipitation	
	R	P*	R	P
Yangtze River Basin	0.82	$P < 0.01$	−0.07	–
Haihe River Basin	0.45	$P < 0.05$	0.34	$P < 0.1$
Heihe River Basin	0.19	–	0.62	$P < 0.01$
Huaihe River Basin	0.55	$P < 0.01$	0.24	–
Yellow River Basin	0.43	$P < 0.05$	0.36	$P < 0.1$
Songhuajiang Basin	0.35	$P < 0.1$	0.4	$P < 0.05$
Zhujiang River Basin	0.81	$P < 0.01$	0.01	–
Tarim River Basin	−0.41	–	0.26	–

*"$P < 0.01$" represents the correlation coefficient is significant at 0.01 level, "–" represents the correlation coefficient is non-significant.

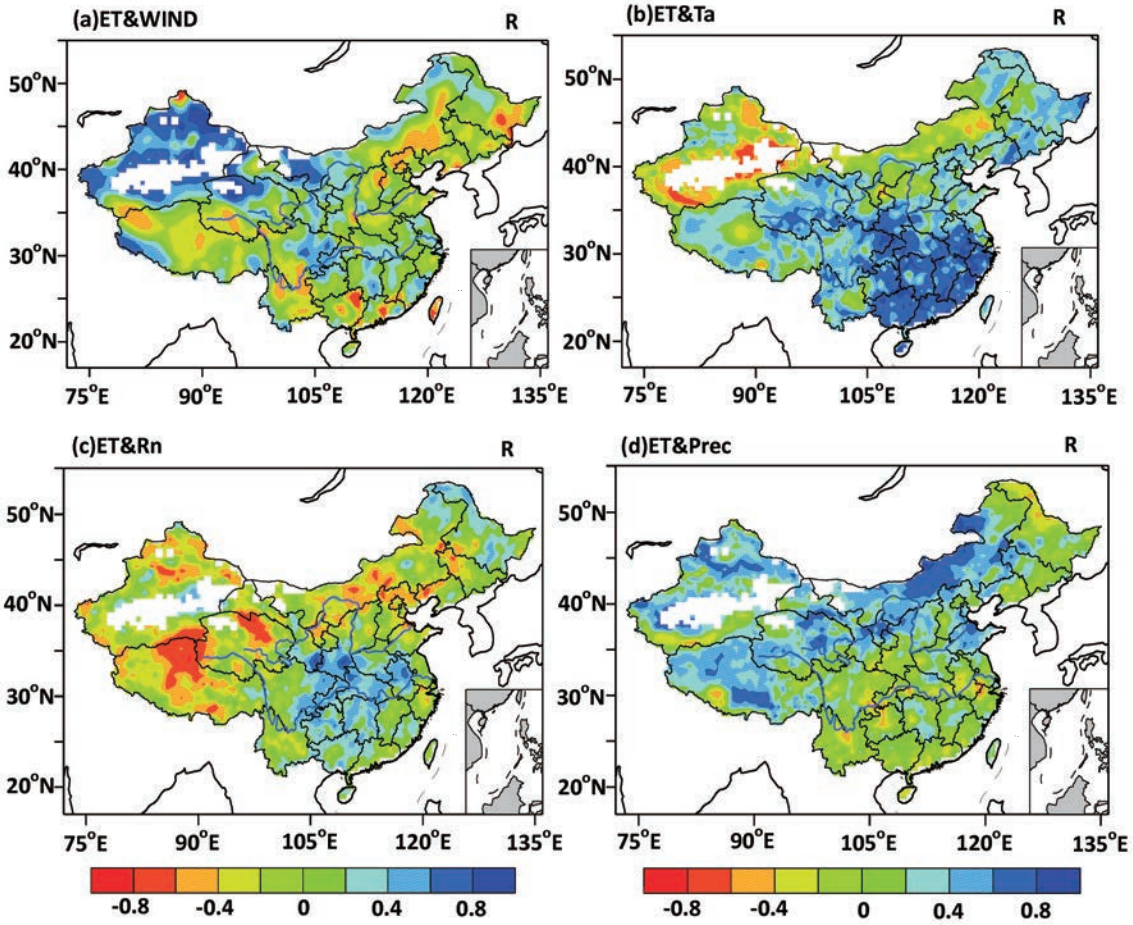

Fig. 8. Spatial distributions of the correlation coefficients for the relationships between annual ET and climate variables: (a) WIND, wind speed; (b) T_a, air temperature; (c) R_n, shortwave radiation; (d) Prec, precipitation. The white area in Northwest China represents the default Obs_MTE values.

basin, and Songhuajiang River basin), where the water availability in the root zone or shallow surface controlled the ET process. It should be noted that ET had the strongest positive correlation with precipitation in the Tarim River basin (most of this area is desert), whereas the correlation coefficient between ET and precipitation in the Tarim River basin was the lowest in the arid and semi-arid areas [Heihe River basin (R = 0.62), Tarim River basin (R = 0.26), Haihe basin (R = 0.34), Yellow river basin (R = 0.36), and Songhuajiang River basin (R = 0.4)]. This could largely be explained by the use of default values for the Obs_MTE data in some areas of the Tarim River basin.

4. Discussion

Land ET is a very important variable for the global hydrological cycle and energy cycle because of land–atmosphere interactions within the climate system. Due to the lack of actual long-term ET observation data, quantifying the spatiotemporal patterns and changes in regional ET are major challenges for the hydrology and climate research community. Thus, in this study, we employed multiple types of forcing and multiple models in an ensemble method to reduce the uncertainties during simulations of the actual ET using land surface modeling, which is a promising method for reproducing high resolution long-term spatial and temporal ET data.

It should be noted that this study had some limitations. First, the use of multiple types of forcing and multiple models in ensemble simulations can reduce some uncertainties, and the ensemble-simulated ET obtained using a simple arithmetical averaging ensemble method (Ens_Mean) captured the spatial patterns and temporal variations very well in China; however, some errors were still present, such as underestimated ET in South China (Figs. 3–6). The simple arithmetical averaging ensemble method is an effective strategy for reducing the uncertainty of individual ensemble members, but it is still inferior to the best individual ensemble member in most cases (Guo et al., 2007).

Therefore, it may be necessary to employ a more advanced ensemble method, such as the Bayesian model averaging (BMA) method (Liu and Xie, 2013). The BMA ensemble method can be applied to multiple types of forcing and multiple models to obtain the ensemble-simulated ET and further reduce the uncertainties, thereby obtaining more accurate actual ET estimates.

Second, in order to evaluate and compare the ensemble-simulated actual ET, we used Obs_MTE data as the ET observations. In fact, the Obs_MTE data comprise estimates of the local ET and meteorological records based on FLUXNET tower and satellite observations. Thus, these data contain errors, e.g., in cold and dry deserts these data do not consider the non-vegetated areas (Jung et al., 2009, 2010). We did not consider the uncertainty of Obs_MTE data in the present study.

5. Summary and conclusion

In this study, we conducted comparisons of six simulations and the Ens_Mean with Obs_MTE over mainland China and the eight major river basins of China during 1982–2007, where we explored the trends and spatiotemporal characteristics of ET, as well as the spatiotemporal pattern of ET in response to climatic factors.

In general, the six simulations and Ens_Mean showed similar broad spatial patterns of ET, with a decrease from southeast to northeast, and then to the northwest, and the lowest annual ET values located in the Tarim River and Heihe River basins of Northwest China. However, there were considerable differences in magnitude among the four LSMs. For example, BATS driven by the Princeton dataset overestimated the mean annual ET for most of the basins, whereas VIC obtained underestimates using the same forcing dataset. Compared with the Obs_MTE product (436 mm yr^{-1}), the Ens_Mean underestimated the annual mean ET in China by 18% (383 mm yr^{-1}); however, the simulated ET exhibited more significant overall variation. In terms of the temporal trend in ET, both the Obs_MTE and Ens_Mean in mainland China exhibited significant increasing trends during 1982–98, whereas the Ens_Mean exhibited a significant decreasing trend during 1998–2007 and the Obs_MTE had a non-significant decreasing trend.

The sensitivity of ET to climate change in this study showed that air temperature was the main factor that controlled the long-term variation in ET over humid areas (e.g., the Yangtze River basin, Huaihe River basin and Zhujiang River basin), whereas precipitation made more of a contribution in arid and semi-arid areas (e.g., the Heihe River basin, Tarim River basin, Haihe River basin, Yellow River basin, and Songhuajiang River basin).

These results suggest that climatic factors such as precipitation and air temperature can have a significant impact on future projections of water cycle dynamics at basin and regional scales.

Acknowledgements. This research was supported by the National Natural Science Foundation of China (Grant Nos. 41405083, 91437220 and 41305066), the Natural Science Foundation of Hunan Province (Grant No. 2015JJ3098), and the Fund Project for The Education Department of Hunan Province (Grant No. 14C0897). We thank Prof. Kun YANG for providing the ITPCAS meteorological forcing data.

REFERENCES

Adler, R. F., and Coauthors, 2003: The Version-2 Global Precipitation Climatology Project (GPCP) monthly precipitation analysis (1979–present). *J. Hydrometeor.*, **4**, 1147–1167.

Bonan, G. B., 2008: Forests and climate change: Forcings, feedbacks, and the climate benefits of forests. *Science*, **320**(5882), 1444–1449.

Chen, J., B. Z. Chen, T. A. Black, J. L. Innes, G. Y. Wang, G. Kiely, T. Hirano, and G. Wohlfahrt, 2013: Comparison of terrestrial evapotranspiration estimates using the mass transfer and Penman-Monteith equations in land surface models. *J. Geophys. Res.*, **118**, 1715–1731, doi: 10.1002/2013JG002446.

Chen, M., P. Xie, J. E. Janowiak, and P. A. Arkin, 2002: Global land precipitation: A 50-yr monthly analysis based on gauge observations. *J. Hydrometeor.*, **3**, 249–266.

Chen, Y., and Coauthors, 2014: Comparison of satellite-based evapotranspiration models over terrestrial ecosystems in China. *Remote Sensing of Environment*, **140**, 279–293, doi: 10.1016/j.rse.2013.08.045.

Chen, Y. Y., K. Yang, J. He, J. Qin, J. C. Shi, J. Y. Du, and Q. He, 2011: Improving land surface temperature modeling for dry land of China. *J. Geophys. Res.*, **116**, D20104, doi: 10.1029/2011JD015921.

Dickinson, R. E., A. Henderson-Sellers, and P. J. Kennedy, 1993: Biosphere-Atmosphere Transfer Scheme (BATS) Version 1e as coupled to the NCAR Community Climate Model. NCAR Tech. Note NCAR/TN387+STR, 77 pp.

Dirmeyer, P. A., 1994: Vegetation stress as a feedback mechanism in midlatitude drought. *J. Climate*, **7**, 1463–1483.

Dirmeyer, P. A., A. J. Dolman, and N. Sato, 1999: The pilot phase of the global soil wetness project. *Bull. Amer. Meteor. Soc.*, **80**(5), 851–878.

Dirmeyer, P. A., X. Gao, M. Zhao, Z. Guo, T. Oki, and N. Hanasaki., 2006: GSWP-2: multi-model analysis and implications for our perception of the land surface. *Bull. Amer. Meteor. Soc.*, **87**, 1381–1397.

Fu, J. L., W. H. Qian, X. Lin, and D. L. Chen, 2008: Trends of graded precipitation days in China from 1961 to 2000. *Adv. Atmos. Sci.*, **25**(2), 267–278, doi: 10.1007/s00376-008-0267-2.

Gao, G., D. L. Chen, C. Y. Xu, and E. Simelton, 2007: Trend of estimated actual evapotranspiration over China during 1960-2002. *J. Geophys. Res.*, **112**, D11120, doi: 10.1029/2006JD008010.

Gao, G., C. Y. Xu, D. L. Chen, and V. P. Singh, 2012: Spatial and temporal characteristics of actual evapotranspiration over Haihe River basin in China. *Stochastic Environmental Research and Risk Assessment*, **26**, 655–669, doi: 10.1007/s00477-011-0525-1.

Giorgi, F., R. Francisco, and J. S. Pal, 2003: Effects of a subgrid-scale topography and land use scheme on the simulation of surface climate and hydrology. Part I: Effects of temperature and water vapor disaggregation. *Journal of Hydrometeorology*, **4**, 317–333.

Guo, Z. C., P. A. Dirmeyer, X. Gao, and M. Zhao, 2007: Improving the quality of simulated soil moisture with a multi-model ensemble approach. *Quart. J. Roy. Meteor. Soc.*, **133**, 731–747.

He, J., 2010: Development of a surface meteorological dataset of China with high temporal and spatial resolution. M.S. thesis, Institute of Tibetan Plateau Research, Chinese Academy of Sciences, Beijing, China. (in Chinese)

Jaksa, W. T., V. Sridhar, J. L. Huntington, and M. Khanal, 2013: Evaluation of the complementary relationship using Noah Land Surface Model and North American Regional Reanalysis (NARR) data to estimate evapotranspiration in semiarid ecosystems. *Journal of Hydrometeorology*, **14**(1), 345–359.

Jung, M., M. Reichstein, and A. Bondeau, 2009: Towards global empirical upscaling of FLUXNET eddy covariance observations: Validation of a model tree ensemble approach using a biosphere model. *Biogeosciences*, **6**, 2001–2013.

Jung, M., and Coauthors, 2010: Recent decline in the global land evapotranspiration trend due to limited moisture supply. *Nature*, **467**, 951–954.

Kalnay, E., and Coauthors, 1996: The NCEP/NCAR 40-year reanalysis project. *Bull. Amer. Meteor. Soc*., **77**, 437–471.

Li, X. L., and Coauthors, 2014: Estimation of evapotranspiration over the terrestrial ecosystems in China. *Ecohydrology*, **7**, 139–149.

Liang, X., and Z. H. Xie, 2001: A new surface runoff parameterization with subgrid-scale soil heterogeneity for land surface models. *Advances in Water Resources*, **24**, 1173–1193.

Liang, X., E. F. Wood, and D. P. Lettenmaier, 1996: Surface soil moisture parameterization of the VIC-2L model: Evaluation and modification. *Global and Planetary Change*, **13**, 195–206.

Liu, J. G., and Z. H. Xie, 2013: Improving simulation of soil moisture in China using a multiple meteorological forcing ensemble approach. *Hydrology and Earth System Sciences*, **17**, 3355–3369, doi: 10.5194/hess-17-3355-2013.

Mao, J. F., and Coauthors, 2015: Disentangling climatic and anthropogenic controls on global terrestrial evapotranspiration trends. *Environmental Research Letters*, **10**(9), 094008, doi: 10.1088/1748-9326/10/9/094008.

Matthews, E., 1983: Global vegetation and land use: New high resolution data bases for climate studies. *J. Clim. Appl. Meteor.*, **22**, 474–487.

Mitchell, K. E., and Coauthors, 2004: The multi-institution North American Land Data Assimilation System (NLDAS): Utilizing multiple CIP products and partners in a continental distributed hydrological modeling system. *J. Geophys. Res.*, **109**, D07S90, doi: 10.1029/2003JD003823.

Niu, G. Y., and Coauthors, 2007: Development of a simple groundwater model for use in climate models and evaluation with gravity recovery and climate experiment data. *J. Geophys. Res.-Atmos.*, **112**, doi: 7110.01029/02006jd007522.

New, M., M. Hulme, and P. Jones, 1999: Representing twentieth-century space–time climate variability. Part I: Development of a 1961–90 mean monthly terrestrial climatology. *J. Climate*, **12**, 829–856.

Oki, T., and S. Kanae, 2006: Global hydrological cycles and world water resources. *Science*, **313**, 1068–1072, doi: 10.1126/science.1128845.

Oleson, K. W., and Coauthors, 2004: Technical description of the community land model (CLM). Tech. Note NCAR/TN-461+STR, Natl. Cent. Atmos. Res., Boulder CO, 174 pp.

Oleson, K. W., and Coauthors, 2007: CLM 3.5 documentation. 34 pp. [Available online at http://www.cgd.ucar.edu/tss/clm/distribution/clm3.5/CLM3_5_documentation.pdf.]

Pinker, R. T., and I. Laszlo, 1992: Modeling surface solar irradiance for satellite applications on a global scale. *J. Appl. Meteor*., **31**, 194–211, doi: 10.1175/1520-0450(1992)031<0194:MSSIFS>2.0.CO;2.

Qian, T. T., A. G. Dai, K. E. Trenberth, and K. W. Oleson, 2006: Simulation of global land surface conditions from 1948 to 2004. Part I: Forcing data and evaluations. *Journal of Hydrometeorology*, **7**, 953–975.

Rodell, M., and Coauthors, 2004: The global land data assimilation system. *Bull. Amer. Meteor. Soc*., **85**, 381–394.

Sheffield, J., G. Goteti, and E. F. Wood, 2006: Development of a 50-year high- resolution global dataset of meteorological forcings for land surface modeling. *J. Climate*, **19**, 3088–3111, doi: 10.1175/JCLI3790.1.

Sheffield, J., and E. F. Wood, 2007: Characteristics of global and regional drought, 1950–2000: Analysis of soil moisture data from off-line simulation of the terrestrial hydrologic cycle. *J. Geophys. Res.*, **112**, D17115, doi: 10.1029/2006JD008288.

Shi, X. Y., J. F. Mao, P. E. Thornton, and M. Y. Huang, 2013: Spatiotemporal patterns of evapotranspiration in response to multiple environmental factors simulated by the Community Land Model, Environ. *Environmental Research Letters*, **8**, 024012, doi: 10.1088/1748-9326/8/2/024012.

Tian, X. J., Z. H. Xie, A. G. Dai, B. H. Jia, and C. X. Shi, 2010: A microwave land data assimilation system: Scheme and preliminary evaluation over China. *J. Geophys. Res*., **115**, D21113, doi: 10.1029/2010JD014370.

Vinukollu, R. K., J. Sheffield, E. F. Wood, M. G. Bosilovich, and D. Mocko, 2012: Multimodel analysis of energy and water fluxes: Intercomparisons between operational analyses, a land surface model, and remote sensing. *Journal of Hydrometeorology*, **13**(1), 3–26.

Wang, A. H., and X. B. Zeng, 2011: Sensitivities of terrestrial water cycle simulations to the variations of precipitation and air temperature in China. *J. Geophys. Res*., **116**, D02107, doi: 10.1029/2010JD014659.

Wang, A. H., D. P. Lettenmaier, and J. Sheffield, 2011: Soil moisture drought in China, 1950–2006. *J. Climate*, **24**, 3257–3271.

Wang, K. C., R. E. Dickinson, M. Wild, and S. L. Liang, 2010: Evidence for decadal variation in global terrestrial ET between 1982 and 2002: 2.Results. *J. Geophys. Res*., **115**, D20113, doi: 10.1029/2010JD013847.

Wang, K. C., and R. E. Dickinson, 2012: A review of global terrestrial evapotranspiration: Observation, modeling, climatology, and climatic variability. *Rev. Geophys*., **50**, RG2005, doi: 10.1029/2011RG000373.

Wei, J. F., P. A. Dirmeyer, and Z. C. Guo, 2008: Sensitivities of soil wetness simulation to uncertainties in precipitation and radiation. *Geophys. Res. Lett*., **35**, L15703, doi: 10.1029/2008GL034494.

Xu, C. Y., L. B. Gong, T. Jiang, D. L. Chen, and V. P. Singh, 2006: Analysis of spatial distribution and temporal trend of reference evapotranspiration and pan evaporation in Changjiang (Yangtze River) catchment. *J. Hydrol*., **327**(1–2), 81–93.

Yang, K., T. Koike, and B. S. Ye, 2006: Improving estimation of hourly, daily, and monthly solar radiation by importing global data sets. *Agricultural and Forest Meteorology*, **137**, 43–55.

Zhang, Y.-C., W. B. Rossow, A. A. Lacis, V. Oinas, and M. I. Mishchenko, 2004: Calculation of radiative fluxes from the surface to top of atmosphere based on ISCCP and other global data sets: Refinements of the radiative transfer model and the input data. *J. Geophys. Res.*, **109**, D19105, doi: 10.1029/2003JD004457.